RAPID COMMUNICATIONS

PHYSICAL REVIEW C VOLUME 47, NUMBER 2 FEBRUARY 1993

Superdeformed band in ^{142}Sm

G. Hackman, S. M. Mullins, J. A. Kuehner, D. Prévost, and J. C. Waddington
Department of Physics and Astronomy, McMaster University, Hamilton, Ontario, Canada L8S 4M1

A. Galindo-Uribarri, V. P. Janzen,* D. C. Radford, N. Schmeing, and D. Ward
AECL Research, Chalk River Laboratories, Chalk River, Ontario, Canada K0J 1J0
(Received 12 November 1992)

Observation of γ-γ coincidences from the reaction ^{124}Sn(^{24}Mg,xn) at 145 MeV has revealed a discrete superdeformed rotational band and evidence of a superdeformed continuum in ^{142}Sm. This result is consistent with cranked shell model calculations indicating shell gaps favorable to superdeformed structures in $N = 80$, $Z \sim 64$ nuclei. It is proposed that the ^{142}Sm band may be described by a proton hole in an ^{143}Eu core. The dynamic moment of inertia of the superdeformed band is more constant than predicted by the model. This may be due to a strong residual interaction between a 6_1 proton intruder and aligning $N = 6$ valence neutrons.

PACS number(s): 21.10.Re, 21.60.Ev, 27.60.+j

Many nuclei in the mass regions $A \sim 135$ and $A \sim 150$ exhibit large quadrupole deformation at high spins with simple integer ellipsoidal axis ratios of $3:2:2$ and $2:1:1$, respectively. Highly deformed shapes are driven by the occupation of high-j intruder orbitals. The properties of high-spin structures in $A \sim 135$ are dominated by one or two neutron intruders from the $N = 6$ major oscillator shell, whereas the $A \sim 150$ superdeformed bands involve a concert of $\pi 6^{2,3,4}\nu 6^{0,\ldots,4}\nu 7^{1,2}$ quasiparticles. Also, while the deformations of the $A \sim 135$ nuclei vary with specific configurations, the $A \sim 150$ superdeformed nuclei all have nearly the same deformation. A question of interest is the high-spin systematics of nuclei intermediate to these regions. Is there a continuous evolution of shape from $A \sim 135$ to $A \sim 150$, or are these regions sharply bounded?

Cranked shell model (CSM) calculations such as those implemented by Nazarewicz *et al.* [1] predict large shell gaps at $N = 80$, $Z = 62, 63, 64$ for superdeformed shapes $\beta_2 \simeq 0.5$. These gaps persist with increasing rotational frequency, hence high-spin superdeformed states in these nuclei should be particularly stable. ^{144}Gd was predicted to be the best case in this region for superdeformation. This nucleus has been studied extensively [2–4], but only recently has a candidate for a discrete superdeformed band been reported [4].

The ^{144}Gd null results are explained in Ref. [1] as a result of a nonconstant moment of inertia. A band crossing from the alignment of a pair of $N = 6$ protons at $\hbar\omega \sim 0.38$ MeV is calculated associated with superdeformation. Standard techniques for uncovering weak superdeformed bands search for a cascade of transitions with constant spacing, which is associated with a constant $\mathcal{J}^{(2)}$. Hence the ^{144}Gd superdeformed band would not be revealed by these techniques.

These same calculations predicted that the shell structure would favor superdeformation in ^{143}Eu. In this case the $N = 6$ proton crossing would be blocked, so the superdeformed ^{143}Eu $\mathcal{J}^{(2)}$ would be more constant than ^{144}Gd. A superdeformed band was indeed discovered in ^{143}Eu [5, 6],[1] and its $\mathcal{J}^{(2)}$ was even more constant than could be explained by proton alignment blocking alone.

The present communication is part of a systematic study of highly deformed bands in nuclei near $N = 80$, namely, ^{141}Gd [7], ^{142}Sm, ^{141}Pm, and ^{144}Eu. We report on a superdeformed band in ^{142}Sm, which like ^{143}Eu exhibits a much more constant $\mathcal{J}^{(2)}$ than is predicted by standard mean-field calculations. This may indicate a strong residual interaction not adequately simulated in the mean-field Hamiltonian. It is proposed that the proton 6_1 intruder is occupied both in ^{142}Sm and ^{143}Eu, and that it interacts strongly with aligning $N = 6$ neutrons to give the observed constant $\mathcal{J}^{(2)}$.

A beam of ^{24}Mg at 145 MeV, provided by the TASCC facility at AECL Chalk River Laboratories, was directed upon two stacked self-supporting $\sim$400 μg/cm^2 ^{124}Sn targets. The γ rays were observed with the 8π spectrometer. Digitized energy signals from the 20 escape-suppressed HPGe detectors were gain and Doppler corrected online. The 71-element bismuth germanate (BGO) inner ball measured γ-ray multiplicity and sum energy. Events with double- and higher-fold HPGe coincidences that satisfied a minimum BGO multiplicity condition were recorded onto magnetic tape. The dominant reaction channels were fusion evaporation by the $6n$ reaction to ^{142}Sm [8] and $7n$ to ^{141}Sm [9]. It was estimated that

*Also at McMaster University, Hamilton, Ontario, Canada L8S 4M1.

[1] This band was previously assigned to ^{142}Eu in [5]; see [6] for clarification.

TABLE I. Gamma-ray energies and intensities for the ^{142}Sm superdeformed band, and rotational frequency and $\mathcal{J}^{(2)}$ dynamic moment of inertia derived from these energies. Due to heavy contamination of the 920 keV doublet, a reliable estimate of the intensity of the superdeformed component could not be obtained (n.a.).

E_γ (keV)	I/I_{981} (%)	$\hbar\omega$ (MeV)	$\mathcal{J}^{(2)}$ ($\hbar^2$MeV^{-1})
799.7(2)	64(11)	0.4149(1)	66.2(4)
860.1(3)	77(12)	0.4451(1)	66.3(4)
920.4(2)	(n.a.)	0.4753(1)	66.1(3)
980.9(2)	100	0.5057(1)	65.7(4)
1041.8(3)	94(18)	0.5360(1)	66.2(4)
1102.2(2)	98(16)	0.5663(1)	65.7(4)
1163.2(3)	92(15)	0.5970(1)	64.6(4)
1225.0(2)	109(13)	0.6277(1)	65.9(4)
1285.7(3)	55(12)	0.6585(1)	63.8(5)
1348.4(4)	54(11)	0.6900(1)	63.3(5)
1411.6(3)	49(11)	0.7215(2)	63.8(6)
1474.3(6)	44(11)	0.7531(2)	62.6(9)
1538.2(7)	34(10)	0.7854(2)	61.2(8)
1603.5(8)	27(10)		

the 6n reaction would populate ^{142}Sm with an excitation energy of 40 MeV and a maximum angular momentum of 69$\hbar$. Events were filtered off-line by requiring a minimum value of summed γ-ray energy equivalent to (when efficiency corrected) $\simeq$ 21 MeV. The resulting γ-γ matrix contained 1.37×10^8 events with a 12 : 1 ratio of ^{142}Sm to ^{141}Sm. There was no consistent evidence in the coincidence data for the presence of ^{142}Pm [10] produced via the *p*5*n* evaporation channel, so such events are limited to < 0.5% relative to ^{142}Sm. An automated search algorithm extracted candidates for superdeformed band cascades with approximately constant energy spacing between 55 and 65 keV. The correlation grid technique embodied in the code BANDAID [11] was also used.

The matrix searches revealed a cascade of twelve mutually coincident γ-ray transitions ranging from E_γ = 800 to 1474 keV with an average spacing of $\simeq$61 keV. Also in coincidence with these γ rays were weak transitions of 1538 and 1604 keV. These fourteen transitions were assigned to a rotational cascade arising from the γ decay of a superdeformed nucleus with $\beta_2 \simeq 0.5$. Since most of the band members were obscured by contaminant peaks in the total projection, narrow gates (4.5 keV) were used and, where appropriate, offset to cover the least polluted portion of the superdeformed peak. The sum of these gates produced the spectrum in Fig. 1(a). The presence of strong transitions in ^{142}Sm at 741 keV ($8^-\rightarrow7^-$) and 677 keV ($14\rightarrow13^-$) [8] has made it impossible to confirm whether the band extends to lower transition energies. Relative intensities of the band members are illustrated in Fig. 1(b). The intensity of the 981 keV transition, which carries the maximum flux of the band, was estimated to be (0.5 ± 0.1)% relative to all ^{142}Sm events. (See Table I.)

The multipolarity of the band was checked with two matrices whose (*x*,*y*) axis correspond to γ rays detected at (±37°,±37°) and (±37°,±79°). Gates were placed on

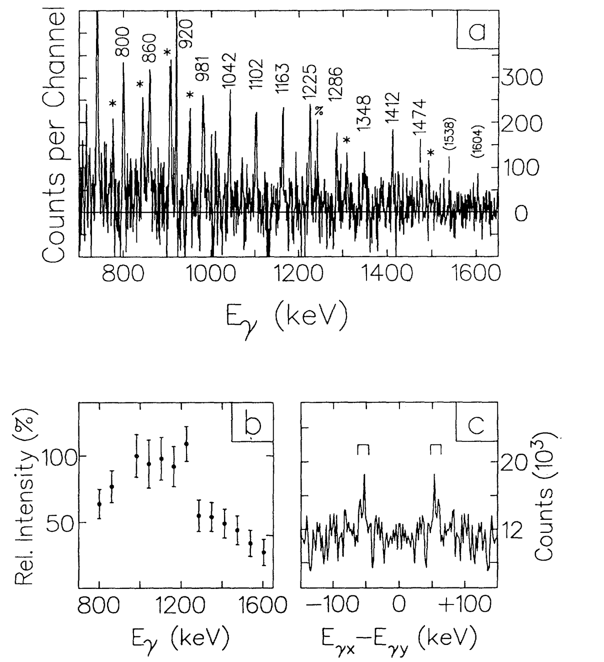

FIG. 1. ^{142}Sm superdeformed band (SDB). (a) Sum of gates spectrum over band members at 800, 860, and 981 to 1474 keV, with * indicating ^{142}Sm transitions and % a ^{141}Sm contaminant. The 920 keV band member is a doublet in coincidence with the $12^+ \rightarrow 10^+$ transition in ^{142}Sm. (b) Intensities relative to the 981 keV band member. The 920 keV transition has been omitted from the intensity plot due to contamination. (c) Ridge structure in the continuum from 1.2 to 1.8 MeV, see text for explanation.

the *x* axis of these matrices and the directional correlation orientation ratios were extracted as $I_y(37°)/I_y(79°)$. This analysis was limited to the γ rays between 981 and 1347 keV, as the remaining band members were too weak in the (±37°,±79°) matrix. The ratios were consistent with those calculated for $E2$-$E2$ correlations and agreed with those measured for an $E2$ cascade in the contaminant ^{141}Sm.

A plot of the $\mathcal{J}^{(2)}$ dynamic moment of inertia versus rotational frequency for the ^{142}Sm and ^{143}Eu superdeformed bands is presented in Fig. 2(a). The $\mathcal{J}^{(2)}$ values are similar at low rotational frequencies, but whereas the ^{143}Eu $\mathcal{J}^{(2)}$ remains constant, the ^{142}Sm $\mathcal{J}^{(2)}$ decreases with increasing $\hbar\omega$. The difference in dynamic moment of inertia ($\Delta\mathcal{J}^{(2)}$) between ^{143}Eu and ^{142}Sm is shown in Fig. 2(b). Theoretical calculations are superimposed and will be discussed below.

In addition to the discrete band, a ridge structure in the γ-γ matrix was observed from 1.2 to 1.8 MeV. Figure 1(c) was generated by projecting a background-subtracted [12] matrix perpendicular to the $E_{\gamma1} = E_{\gamma2}$ line, then subtracting the discrete superdeformed band contributions and any slices which would incorporate other discrete peaks at the energy differences of interest ($\simeq$ 61, 122, etc. keV). The ridge has a full width at half maximum of 12 keV. This would suggest a lower rotational damping than in, for example, ^{149}Gd [13]. However a lower rotational damping should result in promi-

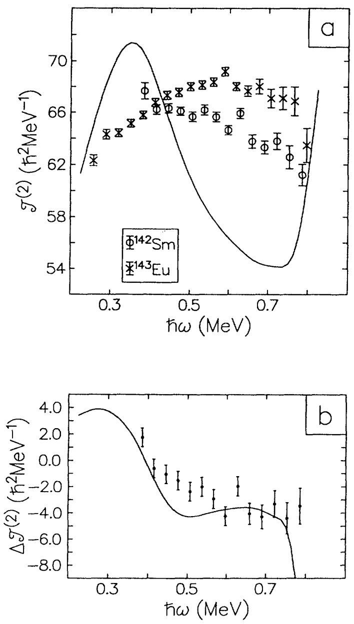

FIG. 2. Dynamic moments of inertia. (a) $\mathcal{J}^{(2)}$ of the superdeformed bands in ^{142}Sm and ^{143}Eu derived from γ-ray energies; (b) $\Delta\mathcal{J}^{(2)} = \mathcal{J}^{(2)}_{\rm Sm} - \mathcal{J}^{(2)}_{\rm Eu}$ calculated by linear interpolation. The solid lines are calculations based on a proposed configuration (see text).

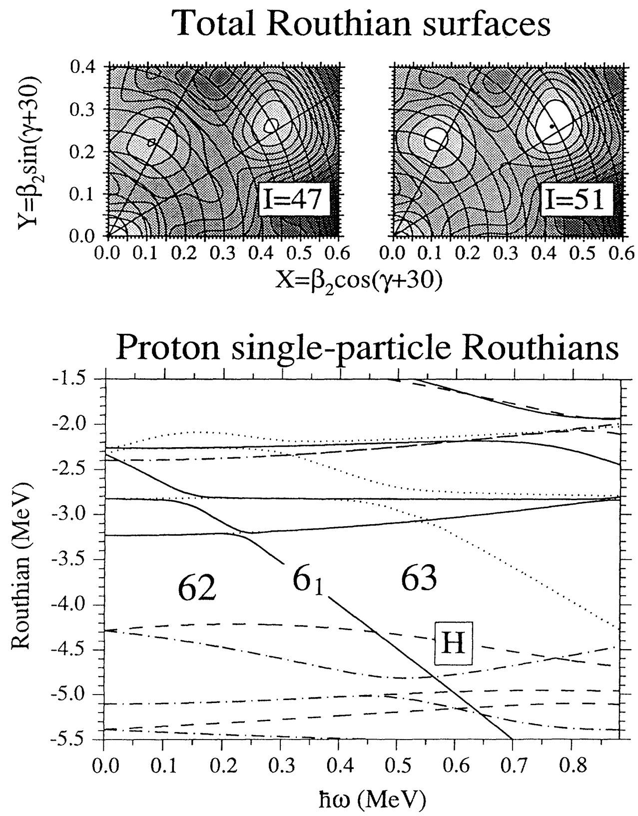

FIG. 3. CSM calculations of total Routhians (top) and proton single-particle levels (bottom). The TRS is calculated for the (–,1) configuration with contour lines separated by 0.6 MeV, and the superdeformed minimum in the $I = 51\hbar$ TRS frame is located at $\beta_2 = 0.49$, $\beta_4 = 0.004$, $\gamma = 2.1$. These parameters were used to calculate the single-particle level plot, on which the 6_1 intruder and the proton number at the gaps are labeled. The configuration proposed in the text involves a hole in the orbital labeled H.

nent higher-order ridges, which were not observed.

The total Routhian surface (TRS) and proton single-particle level plots of Fig. 3 were generated using the codes of Nazarewicz *et al.* [1]. At angular frequencies of $\hbar\omega = 0.59$ and 0.64 MeV, the spins of the $\beta_2 \sim 0.5$ superdeformed minima are estimated to be $I = 47$ and 51, respectively. For even-even nuclei such as ^{142}Sm, the natural combinations of the parity and signature quantum numbers (π,α) are (+,0) or (–,1), corresponding to even parity-even spin and odd parity-odd spin, respectively. The calculated TRS minimum at $\beta_2 \simeq 0.49$ was deeper and more localized in the (–,1) configuration. This minimum became yrast for $I > 50\hbar$, whereas the ^{143}Eu superdeformed minimum is yrast at $I > 35\hbar$. Hence, ^{143}Eu was expected to be fed more strongly, in agreement with experiment.

The configuration for superdeformed ^{143}Eu is $\pi 6^1_1 \nu 6^2_{\Omega=3/2} \nu 7^0$. If the superdeformed ^{143}Eu nucleus is taken as a (π,α)=(+,+$\frac{1}{2}$) magic core,[2] then the superdeformed ^{142}Sm nucleus would have a hole in the (–,–$\frac{1}{2}$) Routhian which is the lower boundary of the Z=63 shell gap between $\hbar\omega \simeq 0.45$ and 0.75 MeV. At $\omega = 0$ this trajectory is a $[541]\frac{1}{2}^-$ Nilsson orbital coming from the $h_{9/2}$ spherical multiplet. The ^{142}Sm proton configuration may then be labeled $^{143}\text{Eu}\otimes\{[541]\frac{1}{2}^-\}^{-1}_{\alpha=-\frac{1}{2}}$ with (π,α) =(–,1) in agreement with the favored TRS minimum. The energy splitting from the $\alpha = +\frac{1}{2}$ component is sufficient to explain the lack of an observed signature partner. The $\pi 6_1$ intruder drives the ^{143}Eu and ^{142}Sm nuclei to higher deformation than the $A \sim 135$ nuclei, but not as high as the $A \sim 150$ $\nu 7^{1,2}$ superdeformed nuclei. Ongoing analysis of high-spin states in the intermediate region should clarify the situation, especially ^{144}Eu which should be the lightest isotope with a $\nu 7$ intruder.

Figure 2(a) shows the results of a calculation of the SD band $\mathcal{J}^{(2)}$ dynamic moment of inertia with particle number projected pairing and the renormalized macroscopic radius described in [1]. The experimentally observed $\mathcal{J}^{(2)}$ is more constant in ω than the theoretical prediction. This was also the case with ^{143}Eu [5]. In both cases, the $\mathcal{J}^{(2)}$ decreases with increasing ω following a bump at $\hbar\omega \simeq 0.38$ MeV caused by the alignment of $N = 6$ neutrons with a very strong interaction [1]. The discrepancies between theory and experiment may result from an inadequate treatment of n-p correlations in the mean-field Hamiltonian. Studies of high-j intruder bands in the $A \sim 110$ [14], ~ 135 [15], and ~ 170 [16]

[2]The single-particle Routhians suggest ^{143}Eu is a double-closed-shell magic core (see [1] for details). This is consistent with the observed constant $\mathcal{J}^{(2)}$ dynamic moment of inertia.

mass regions indicate that an intruder particle perturbs the alignment of a high-j pair of opposite character, e.g., $\pi h_{11/2}$ and $\{\nu h_{11/2}\}^2$ in ^{113}Sb [14]. This interaction is strongest when the orbitals come from the same subshell and have equal or similar K quantum numbers. In ^{142}Sm and ^{143}Eu, the aligning $N = 6$, $\Omega = \frac{3}{2}$ neutrons may interact strongly with the $\pi 6_1$ intruder. The $\nu 6$ energy levels would be repelled and the $\mathcal{J}^{(2)}$ would be less perturbed than without the n-p interaction.

The difference between the calculated $\mathcal{J}^{(2)}$ for ^{142}Sm and ^{143}Eu is superimposed on the experimental $\Delta\mathcal{J}^{(2)}$ in Fig. 2(b), the latter being derived by linear interpolation. Assuming that any changes in pairing are negligible, this should demonstrate the contribution of the negative parity hole in ^{142}Sm. The theoretical and experimental $\Delta\mathcal{J}^{(2)}$ agree much better (within $\sim 2\sigma$) than the $\mathcal{J}^{(2)}$ values alone.

In summary, a superdeformed band has been found in the N=80 nucleus ^{142}Sm. The band has a similar energy spacing ($\sim$61 keV) to the one belonging to the isotone ^{143}Eu. The maximum intensity of the band relative to the total decay flow into ^{142}Sm was estimated to be (0.5 $\pm$ 0.1)%. There is also evidence for a superdeformed continuum, since a ridge is observed. Comparison with cranked Woods-Saxon calculations suggest that the band can be interpreted as a negative parity proton hole configuration in the ^{143}Eu core, namely $\pi 6^1 \nu 6^2 \nu 7^0 \otimes \{[541]\frac{1}{2}^-\}^{-1}_{\alpha=-\frac{1}{2}}$. The corresponding (–,1) total Routhian surface shows a superdeformed minimum ($\beta_2 \simeq 0.49$) which is yrast at $\sim 50\hbar$. The $\mathcal{J}^{(2)}$ dynamic moment of inertia decreases with increasing frequency whereas the ^{143}Eu $\mathcal{J}^{(2)}$ remains constant. Standard mean-field calculations, however, predict a much steeper down slope in ^{142}Sm $\mathcal{J}^{(2)}$ following the alignment of the $N = 6$ neutron pair. The calculations fail in a similar fashion for ^{143}Eu. A possible explanation is that a strong residual interaction between the 6_1 proton intruder and the $N = 6$ neutrons perturbs the alignment, smoothing out the $\mathcal{J}^{(2)}$. Even so, the differences in $\mathcal{J}^{(2)}$ between ^{142}Sm and ^{143}Eu are remarkably well reproduced by taking the differences between the calculations.

Dr. R. A. Wyss is thanked for his guidance and assistance with the calculations. The crew and staff at TASCC are thanked for supplying the beam. This work was partially supported by the Natural Sciences and Engineering Research Council of Canada (NSERC).

---

[1] W. Nazarewicz, R. Wyss, and A. Johnson, Nucl. Phys. **A503**, 285 (1989).
[2] J. P. Vivien *et al.*, Phys. Rev. C **33**, 2007 (1986).
[3] Y. Schutz *et al.*, Phys. Rev. C **35**, 384 (1987).
[4] K. Strähle *et al.*, Proceedings of the International Conference on Nuclear Structure at High Angular Momentum, Ottawa, 1992, edited by D. Ward and J. C. Waddington (Report No. AECL-10613, 1992), Vol. II, p.194.
[5] S. M. Mullins *et al.*, Phys. Rev. Lett. **66**, 1677 (1991).
[6] A. Ataç *et al.*, in *Progress in Particle and Nuclear Physics*, edited by A. Faessler (Pergamon, New York, 1991), Vol. 28.
[7] S. M. Mullins *et al.*, in Ref. [4], p. 250.
[8] M. Lach, J. Styczen, R. Julin, M. Piiparien, H. Buescher, P. Kleinheinz, and J. Blomqvist, Z. Phys. A **319**, 235 (1984); Nucl. Data Sheets **63**, 701 (1991).
[9] M. A. Cardona, G. de Angelis, D. Bazzacco, M. De Poli, and S. Lunardi, Z. Phys. A **340**, 345 (1991).
[10] L. Funke, W. D. Fromm, H. J. Keller, R. Arlt, and P. M. Gopytsch, Nucl. Phys **A274**, 61 (1976).
[11] J. A. Kuehner (unpublished).
[12] G. Palameta and J. C. Waddington, Nucl. Instrum. Methods **A234**, 476 (1985).
[13] J. P. Vivien *et al.*, Phys. Lett. B **278**, 407 (1992).
[14] V. P. Janzen *et al.*, in [4], p. 333.
[15] P. H. Regan *et al.*, Phys. Rev. C **42**, 1805 (1990).
[16] L. Hildingsson *et al.*, Nucl. Phys. **A513**, 394 (1990).